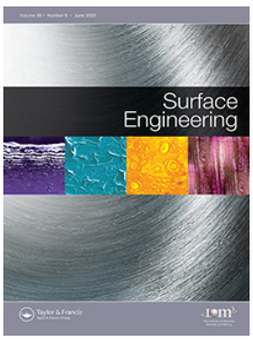

Surface Engineering

ISSN: 0267-0844 (Print) 1743-2944 (Online) Journal homepage: https://www.tandfonline.com/loi/ysue20

Aluminium films roughened by hot water treatment and derivatized by fluoroalkyl phosphonic acid: wettability studies

Yongmao Hu, Ruheng Li, Xueqing Zhang, Yan Zhu & Heng-Yong Nie

To cite this article: Yongmao Hu, Ruheng Li, Xueqing Zhang, Yan Zhu & Heng-Yong Nie (2020) Aluminium films roughened by hot water treatment and derivatized by fluoroalkyl phosphonic acid: wettability studies, Surface Engineering, 36:6, 589-600, DOI: 10.1080/02670844.2019.1647374

To link to this article: https://doi.org/10.1080/02670844.2019.1647374

Published online: 28 Jul 2019.

SURFACE ENGINEERING
2020, VOL. 36, NO. 6, 589–600
https://doi.org/10.1080/02670844.2019.1647374

The Institute of Materials, Minerals and Mining

Taylor & Francis
Taylor & Francis Group

Aluminium films roughened by hot water treatment and derivatized by fluoroalkyl phosphonic acid: wettability studies

Yongmao Hu[a,b], Ruheng Li[a], Xueqing Zhang[a], Yan Zhu[c] and Heng-Yong Nie [b,d]

[a]College of Engineering, Dali University, Dali, People's Republic of China; [b]Surface Science Western, The University of Western Ontario, London, Canada; [c]Faculty of Materials Science and Engineering, Kunming University of Science and Technology, Kunming, People's Republic of China; [d]Department of Physics and Astronomy, The University of Western Ontario, London, Canada

ABSTRACT

Aluminium (Al) films roughened by hot water treatment were used to investigate the impact of their roughness on hydrophobicity upon their derivatization via self-assembled monolayers (SAMs) of a fluoroalkyl phosphonic acid (FPA). Superhydrophobicity was achieved for FPA-derivatized Al films that had been treated in hot water briefly (e.g. 60–180 s), while for prolonged treatment times (e.g. beyond 240 s) degraded hydrophobicity was observed. The observed degradation of hydrophobicity is attributed to surface morphology changes causing water to enter the pores of the roughened Al films. Also studied is the surface chemistry of the FPA SAMs derivatized on Al films, including their thermal stability and a possible mechanism that improves the hydrophobicity. Our results demonstrate that an Al surface immersed in hot water for a couple of minutes generates a porous morphology suitable for rendering superhydrophobicity upon derivatization of the robust FPA SAMs.

ARTICLE HISTORY
Received 4 January 2019
Revised 28 June 2019
Accepted 18 July 2019

KEYWORDS
Roughened Al film in hot water; surface morphology; surface chemistry; fluoroalkyl phosphonic acid; self-assembled monolayers; superhydrophobicity

Introduction

Aluminium (Al) and its alloys have been widely used in architecture, transmission lines, electronic components, micro- and nano-technological systems, and digital micromirror devices [1–6]. Because of the ubiquitous surface contamination and corrosion [7–9], superamphiphobic Al surfaces with functions of self-cleaning, anti-corrosion and anti-icing have gained extensive interests [10–18]. It is well known that Al is easily oxidized in air, resulting in surface energy of 2.64 J m^{-2} for α-Al_2O_3 and 1.67 J m^{-2} for γ-Al_2O_3, respectively [19]. The two steps necessary to achieve superamphiphobicity are (a) construction of micro/nano structures to trap air at the Al/liquid interfaces and (b) modification of the Al surface with chemicals having a low surface energy [20,21]. It had been demonstrated that, from a structural point of view, appropriate microscale structures were favourable for superhydrophobicity. However, superamphiphobicity could only be achieved on surfaces with re-entrant or micro/nanoscale hierarchical structures [13,14,22–24].

On the other hand, studies on wettability of surfaces whose morphology is characterized by nanoscaled structures are scarce. It would be advantageous if a porous surface could be easily made and was suitable for providing superhydrophobicity upon appropriate surface derivatization. This is achievable for Al because it is highly reactive in hot water, leading to the formation of a porous oxide [25,26]. We make use of porous aluminium oxide in preparing superhydrophobic surface via formation of self-assembled monolayers (SAMs) of a fluoroalkyl phosphoric acid (FPA). We use atomic force microscopy (AFM) to estimate the roughness of Al films roughened by hot water treatment and compare their wettability upon derivatization of FPA using contact angle measurements. This way, the impact of the roughness of the Al films on wettability can be determined, which is important in understanding superhydrophobicity.

SAMs of organophosphonic acids, especially octadecylphosphonic acid (OPA), have long been used to modify Al surfaces for ultra-repellency [13,14,22], lubrication and anti-corrosion [27,28]. These systems rely on the ease of formation of the robust P-O–Al linkage as a result of the condensation reaction between the hydroxyl groups of the phosphonic acid headgroups and those of the oxide layer of Al films [13,14,29]. The introduction of fluorocarbon groups in the alkyl chains of the phosphonic acid molecules significantly improves not only the liquid repellency, but also the stability of the SAMs compared to those consisting of only hydrocarbon chains [30]. It has been demonstrated that time-of-flight secondary ion mass spectrometry (TOF-SIMS) is powerful in probing surface chemistry of SAMs [29,31]. TOF-SIMS is uniquely suited to differentiate intact OPA molecules from those altered, which no longer have a chance to be fragmented as a dehydrogenated molecular ion [29]. In present work, the thermal

CONTACT Heng-Yong Nie hnie@uwo.ca Surface Science Western, The University of Western Ontario, 999 Collip Circle, London, Ontario, Canada N6G 0J3; Department of Physics and Astronomy, The University of Western Ontario, London, Ontario, Canada N6A 3K7

stability of FPA SAMs on Al surfaces as a function of annealing temperature was examined using TOF-SIMS and measurements of contact angles (CAs). Those two surface sensitive techniques are capable of probing changes in surface chemistry of the FPA SAMs that are a result of structural changes due to annealing.

Experimental

Materials and sample preparation

Figure 1 illustrates the preparation steps for derivatization of nano-structured Al films and characterization techniques employed. A 15-nm thick Al film with a roughness of 0.4 nm was coated on a clean Si (100) wafer by radio frequency magnetron-sputtering. The Al/Si wafer was cut into coupons (1 cm × 1.5 cm), which were cleaned by being sequentially rinsed with acetone, methanol and deionized (DI) water with a resistivity of 18.2 MΩ·cm (Milli-Q). Nano-structured Al films were prepared by immersing the coupons in DI water maintained at 90°C for different times followed by being dried using a N_2 gas stream.

The FPA used in this study, *1H*, *1H*, *2H*, *2H*-perfluoro-*n*-hexadecylphosphonic acid, $CF_3(CF_2)_{13}(CH_2)_2$-$P(=O)(OH)_2$, was ordered (Proposal SP SSW 04) from Specific Polymers (Castries, France). The crystalline FPA powder was preheated to 100°C (in air) for several minutes prior to use to eliminate moisture. A 1 mM FPA solution in a mixed solvent of methanol and chloroform (with a volume ratio of 1 : 1) was used to derivatize Al surfaces. It is worth mentioning that the FPA molecules were not dissolved completely at this level of concentration at room temperature. When the solution was heated up to 50°C, the FPA was completely dissolved. Derivatization was done by immersing the Al coupons in the FPA solution for 10 h at room temperature to ensure sufficient reactions between the Al surfaces and FPA molecules [32–34]. The FPA/Al samples were then rinsed with methanol and DI water and dried using a N_2 gas stream.

In order to survey the thermal stability and the surface chemistry of the FPA SAMs on the Al films, 16 FPA/Al samples were prepared by immersing the Al/Si substrate in DI water for 120 s at 90°C, followed by FPA derivatization. Two of these 16 samples were used as a control and the other 14 samples were divided into seven sets (two samples for each set). The seven sets of samples were annealed at 100, 150, 200, 250, 300, 350 and 400°C for 15 min on a hot plate in air, respectively. Then, these 16 samples were divided into two sets and each of them included the control and seven annealed samples. One set of the samples was subjected to CA measurements and the other to TOF-SIMS analyses.

Characterizations of surface morphology

The dynamic force mode of a Park Systems XE-100 AFM was used to examine the morphology of the Al films. Cantilevers with a nominal spring constant of 40 N m^{-1}·and resonant frequency of 300 kHz were vibrated and the reduced amplitude was used as the feedback parameter to follow the surface morphology of the samples. The nominal radius of the tip located at the free end of the cantilever was 10 nm. AFM images with a pixel density of 256 × 256 were collected at a scan rate of 1 Hz at room temperature and a relative humidity of 40%. For each sample, at least three areas of 10 μm × 10 μm were scanned, from which the average surface roughness was estimated.

Scanning electron microscopy (SEM, Hitachi SU8020, Japan) was also used to look at the surface structure of 35-nm thick Al films deposited on a Si substrate to confirm/complement the AFM observations. The samples were coated with platinum thin films (~3 nm) to avoid sample charging for SEM imaging. An electron beam was thermionically emitted from an electron gun fitted with a tungsten filament cathode driven by 3 kV.

Wettability studies

CAs of sessile drops of water, methanol and hexadecane on the surface of the FPA/Al samples were

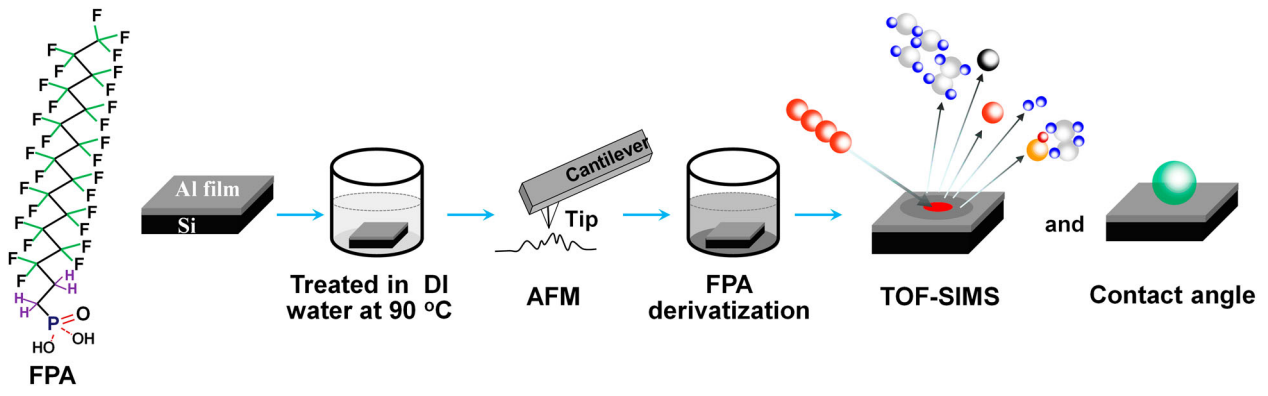

Figure 1. A schematic diagram for preparation and characterization of FPA/Al samples.

measured using a ramé-hart CA goniometer (Model 100-00). The volume of the probing liquid used for CA measurements was ~5 μL, corresponding to a droplet of a diameter of ~2 mm. For each FPA/Al sample, at least three spots were tested and the average CA and the standard deviation were estimated.

Analyses of surface chemistry

An ION-TOF TOF-SIMS IV equipped with a Bi liquid metal ion gun was employed to investigate the surface chemistry of the FPA/Al samples. A pulsed, 25 keV Bi_3^+ cluster primary ion beam (with a pulse width of ~1 ns and a target current of ~1 pA) was used to bombard the sample surface to generate secondary ions. Either positive or negative secondary ions were extracted by an electric field with an appropriate polarity, mass separated and detected via a reflectron-type of time-of-fight analysing system. The base pressure of the analytical chamber was approximately 1×10^{-7} mbar. The cycle time for the primary ion beam bombardment and the detection of the secondary ions was 100 μs. A low energy (~18 eV) pulsed electron flood was used to neutralize sample charging. For each sample, negative and positive secondary ion mass spectra were collected on three spots from 128 × 128 pixels over an area of 200 μm × 200 μm. Negative ion spectra were calibrated using C^-, C_4H^- and CF_3^-, while positive ones using C^+, $C_3H_5^+$ and $C_3F_5^+$. The mass resolutions for ion fragments of C_2H^-, PO_3^-, $C_2H_5^+$ and $C_3H_5^+$ were 3600, 5700, 4300 and 7400, respectively.

Poisson-corrected intensities of characteristic ions were used to study surface chemistry of the FPA SAMs subjected to annealing.

Results and discussion

The morphology of the Al surfaces

Figure 2 shows AFM images of the control and Al films treated in DI water maintained at 90°C for 5, 20, 50, 180 and 720 s, respectively. The control (Figure 2(a)) shows the typical morphology of a sputter-coated metal film, having a root mean squared roughness of 0.4 nm. We confirmed that the derivatization of an FPA monolayer, whose thickness would be on the order of 2 nm if the molecules were fully extended, did not change the morphology of the Al surface. As shown in Figure 2(b), pinholes with a diameter and depth of ~300 and ~5 nm, respectively, were observed upon hot water treatment for 5 s, revealing that the Al film was etched. This resulted in a roughness of 0.6 nm, which is only a slight increase in comparison with that (0.4 nm) of the pristine Al film. When an Al film was treated for 20 s in hot water, the surface was characterized by fewer but larger pinholes (Figure 2(c)), with an increased roughness of 1.1 nm, indicating that the surface was further etched. A jump of roughness to 17.2 nm was observed when an Al film was subjected to hot water treatment for 50 s (Figure 2(d)). With further increased treatment times of 180 s (Figure 2(e)) and 720 s (Figure 2(f)), the roughness is 17.1 and 19.5 nm, respectively.

In order to have an idea as to how the surface of the Al films changed as a function of immersion time in hot water, we present in Figure 3 representative profiles isolated from each of the six AFM images shown in Figure 2. As clearly shown in Figure 3, for Al films treated with hot water for 50 s and beyond, their corrugations are several tens of nanometres, which is an

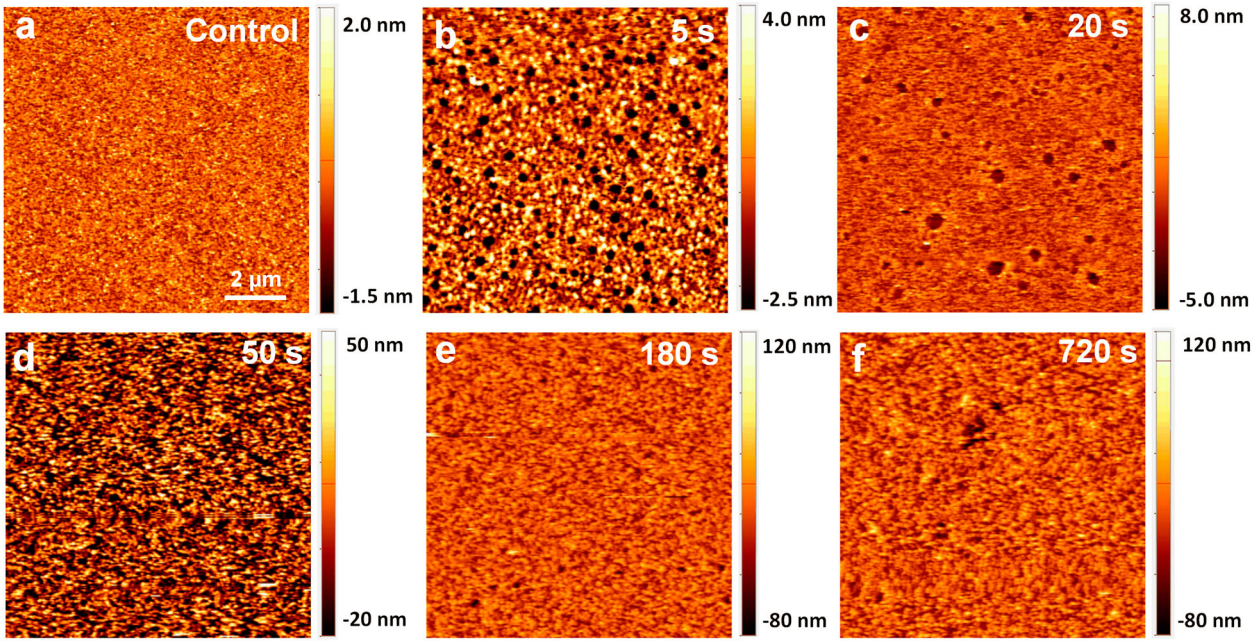

Figure 2. AFM images (10 μm × 10 μm) of the control (a) and Al films treated in DI water maintained at 90°C for 5 (b), 20 (c), 50 (d), 180 (e) and 720 s (f), respectively.

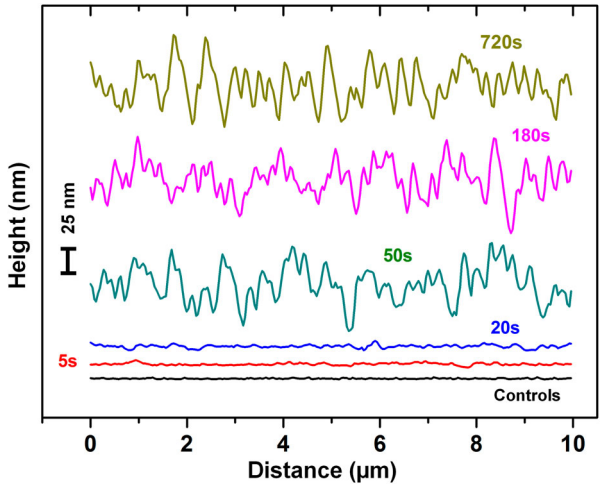

Figure 3. A typical profile for the control and each of the Al films subjected to hot water treatment for 5, 20, 50, 180 and 720 s. The profiles are isolated from the AFM images shown in Figure 2.

enormous increase from that of the control (a couple of nanometres). It is intriguing that these corrugations of several tens of nanometres are much larger than the thickness of the pristine Al film, which is only 15 nm. This experimental observation prompted us to study the thickness increase in Al films subjected to hot water treatment.

In order to measure the thickness of the Al film treated in hot water for 50 s, we collected an AFM image (Figure 4(a)) at a step generated by scratching the Al film using stainless tweezers. The scratching did not damage the hard Si substrate, as confirmed by a similar scratching experiment carried out on the pristine, 15-nm thick Al film (Figure 4(b)). The profile isolated from the AFM image of the pristine Al film, shown in Figure 4(b), revealed the known Al film thickness of 15 nm. This verifies that we completely removed the Al film without damaging the Si substrate. It is clear from the profiles shown in Figure 4(a,b) that the apparent thickness of the treated Al film is roughly 10 times larger than the thickness of the pristine Al film. As shown in the profile in Figure 4(a), the distance between the highest and lowest points probed in the film is roughly 100 nm. This may be explained by the tip effect of AFM, that is, the AFM tip cannot reach the pores that are smaller than the size of the tip [35]. The pyramid-shaped AFM tip, with a cone angle approximately 50°–60°, has a radius of 10 nm at the apex, preventing them from probing narrower columns. This is the reason the AFM tip could not probe more than 100 nm into the film, due to the rather small size of the porous Al film formed in the hot water. If there are lager openings in the film, such as the star-shaped feature located at the lower right corner of the AFM image in Figure 4(a), the AFM tip did reach the Si substrate.

The roughness estimated from the AFM images obtained on the control and Al films treated in hot water is summarized in Figure 5. The roughness shows a surge for Al films treated for 30 s in hot water and plateau thereafter. This experimental observation suggests that one only needs to immerse an Al film in hot water for approximately one minute to achieve a roughness of ~18 nm (as estimated from AFM images of an area of 10 μm × 10 μm).

Hot water treatment of Al and its alloys was originally adopted to enhance the interfacial adhesion

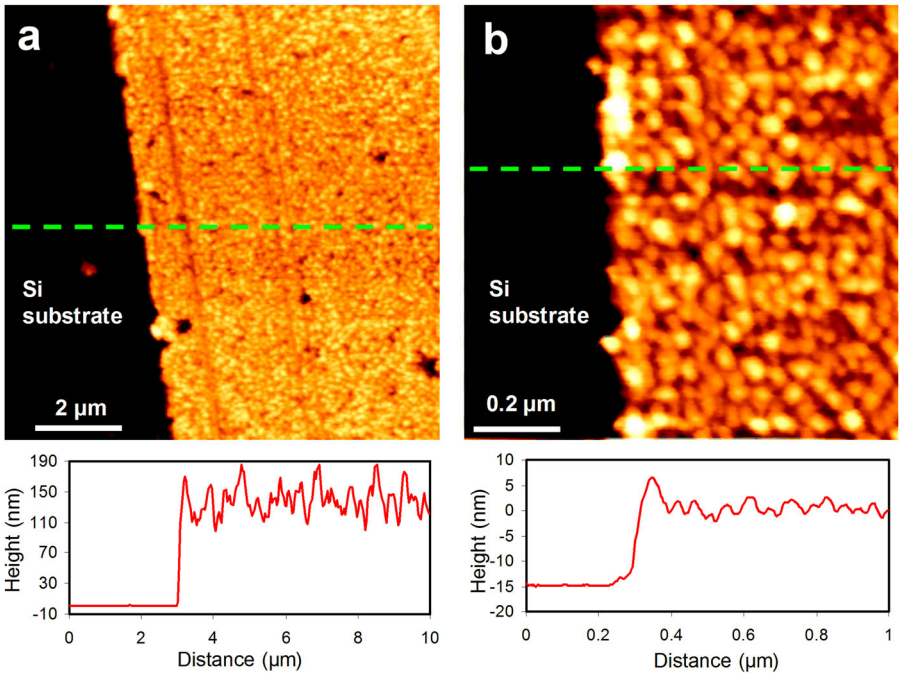

Figure 4. An AFM image and a profile isolated from the image (indicated by the insert line) for (a) an Al film subjected to hot water treatment for 50 s and (b) a pristine Al film.

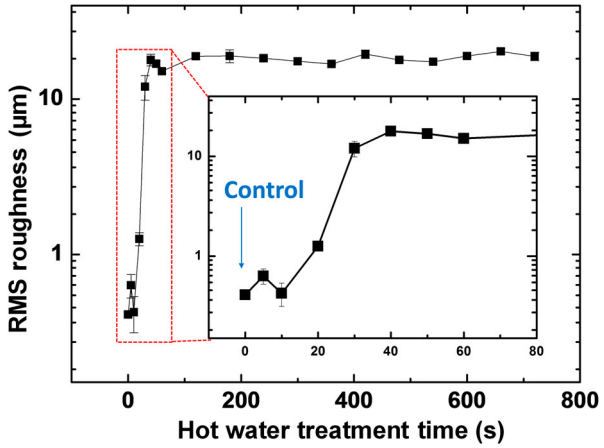

Figure 5. Al surface roughness as a function of treatment time in hot water. The insert shows details of the roughness change for Al films subjected to treatment for the shorter times ranging from 0 to 60 s. The roughness increases rapidly during treatment time of 10–30 s, beyond which it plateaus.

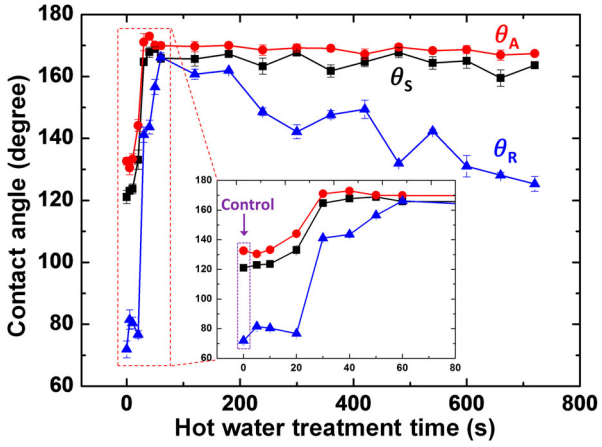

Figure 6. Static, advancing and receding water contact angles as a function of hot water treatment time. The insert details changes in shorter treatment times from 0 to 60 s, where the standard deviations are omitted.

between epoxy and Al joints [36]. Recently, nanoscale roughness of Al and its alloys created via hot water treatment has received extensive attention for modifying surface wettability [37,38]. Alwitt [39] reported that pseudoboehmite oxide film grew on Al in water at temperatures of 50–100°C. The growth process of the pseudoboehmite oxide film was defined in three stages, i.e. incubation (1–2 s), rapid growth and slow growth within the first few minutes of soaking. It is believed that the reaction starts with the dissolution of Al, followed by the deposition of hydroxide colloidal particles to form nanoscale textures. The reactions between Al and H_2O can be described as follows [26,40–42].

$$2Al + 3H_2O \rightarrow Al_2O_3 + 3H_2 \uparrow \quad (1)$$

$$Al^{3+} + O^{2-} + OH^- \rightarrow AlO(OH) \quad (2)$$

Wettability studies of the FPA/Al surfaces

Water, hexadecane and methanol were used to probe the wettability of the FPA/Al samples. The static, advancing and receding water CAs were shown in Figure 6. For the control (i.e. the sample without treatment), the water static CA (θ_S) was 121°, which is typical for water droplets on a smooth surface derivatized with densely packed perfluorocarbons [43]. Meanwhile, the advancing (θ_A) and receding angles (θ_R) of the control were 131° and 72°, respectively. This presents a rather large hysteresis of 59° between the advancing and receding CAs. When the treatment time was raised to 40 s, θ_S, θ_A and θ_R increased monotonously to 168°, 173° and 144°, respectively, and the corresponding hysteresis of advancing and receding CAs decreased to 29°. It is clear from Figure 6 that θ_S fluctuate within the range of 160° to 169° for FPA SAMs prepared on Al films treated in hot water for 40–720 s.

For Al films subjected to hot water treatment for 50–180 s, the hysteresis of the advancing and receding water CAs are below 10°. In fact, during CA measurement we noticed that water droplets easily slipped away from the surface of these FPA/Al samples. This indicates that the water-FPA/Al system is in the Cassie–Baxter regime [44], that is, the composite wetting on a chemically heterogeneous surface where one component is the rough, FPA-derivatized Al surface and the other the air trapped in the pores of the rough surface.

It is interesting to note that further increases in treatment time (240–720 s) resulted in decreased receding CAs and largely unchanged advancing and static CAs. Such an increased CA hysteresis leads to degradation of superhydrophobicity of the FPA/Al surfaces. This observation of reduced receding contact angles, along with the fact that the roughness is underestimated due to the inherent tip effect, indicates that the differences in porosity might not be picked up by AFM. The surface morphology of the treated Al films, characterized by sharp edges of aluminium oxide, is a hard one for AFM because the inherent tip effect of the mechanical probe technique. Moreover, because AFM roughness and morphology did not apparently correlate to the wetting properties of the decreased receding CAs observed, we turn to SEM to seek new information that can further our understanding on the reason for the observed receding CAs variations. Shown in Figure 7(a,b) are SEM images of the surface of a 50-s and a 720-s treated Al film, respectively. We also confirmed that the Si substrate was not affected by the hot water treatment, as evidenced by the cross-section SEM images (Figure 7(c)) of a 35-nm Al film on a Si substrate and a witness Si substrate before and after they were treated in hot water for 720 s. As clearly shown in Figure 7(c), while the Al film measures approximately 400 nm in thickness upon

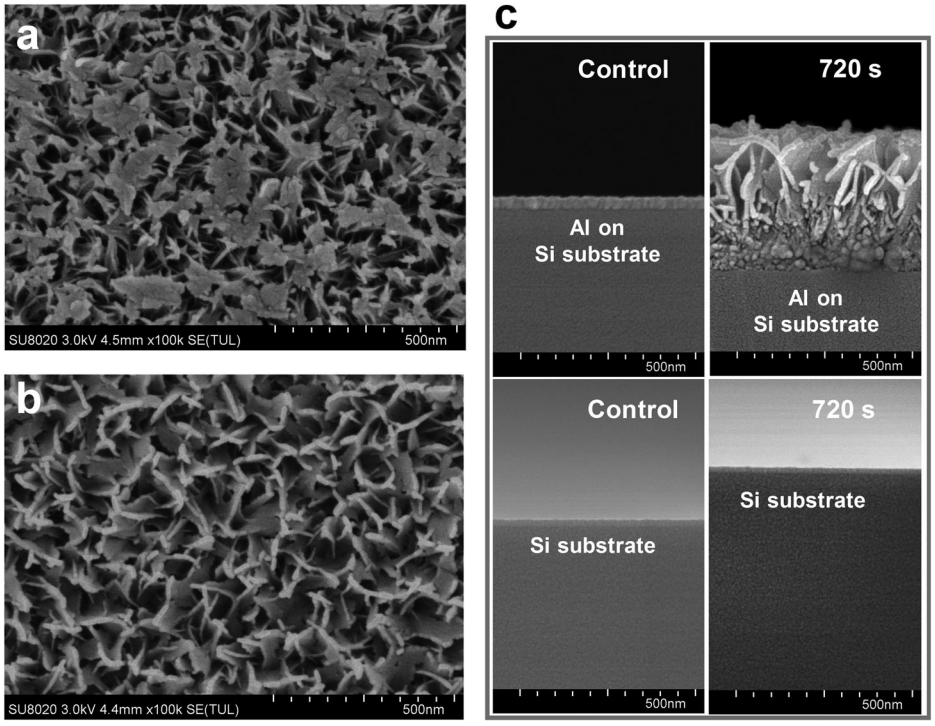

Figure 7. An SEM image of an Al film subjected to hot water treatment for (a) 50 s and (b) 720 s. Shown in (c) are cross-section SEM images of a 35-nm Al film on a Si substrate and a Si substrate witness before and after a 720-s hot water treatment.

the hot water treatment, no changes are seen on the witness Si substrate.

The flat 'areas' (Figure 7(a)) on the surface provides a structure for water droplets to stay on the 50-s treated Al film, while the 720-s treated one has features that are funnel-shaped (Figure 7(b)). Upon FPA derivatization, we believe that it is harder to hold air trapped inside the pores of the 720-s treated Al film. The 50-s treated one is more suitable because it prevents water from entering the pores. The flat areas over the surface of the 50-s treated Al film serve to support the water droplets and the pores in the film from filling with air so that the water droplets are in the Cassie–Baxter regime. By contrast, the surface of the 720-s treated Al film has no such a flat area, rather, it is characterized by funnel-like features with the 'walls' appearing rather smooth. It can be inferred that this structure is less effective in preventing water from entering into the pores. The water droplet on such a surface is likely in the Wenzel regime [45], where water is in contact with the FPA-derivatized surface without air trapped in the pores (thus the surface under the water drop is chemically homogeneous). We can then conclude that the morphology of the Al film with prolonged hot water treatment prefers the Wenzel regime over the Cassie–Baxter one, which should be avoided in the context of realization of superhydrophobicity.

As shown in Figure 8, the static CAs of hexadecane and methanol were also examined. For FPA SAMs prepared on Al films that were treated in hot water for up to 20 s, the hexadecane CAs are in the range of 60°–67°, which is the case when the SAMs were formed on a

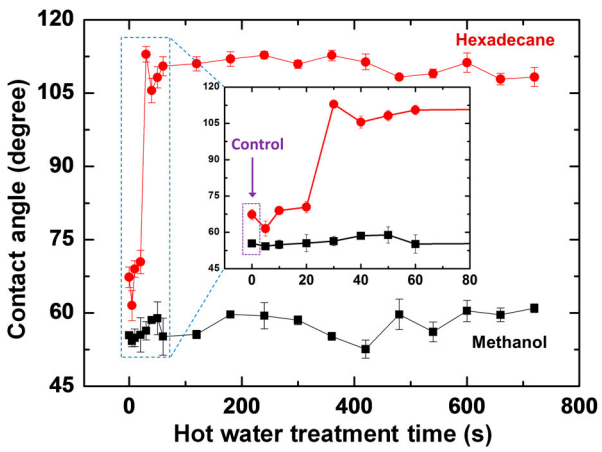

Figure 8. Static hexadecane and methanol contact angles as a function of hot water treatment time. The insert shows the details in the first 60 s.

smooth surface. However, for FPA SAMs made on an Al film treated in hot water for 30 s, there is a burst in the hexadecane CA, reaching 113°. This burst in CA coincides with the roughness surge shown in Figure 5. However, for longer treatment times, there are no significant changes in hexadecane CAs. This trend agrees with that of static water CAs shown in Figure 6. Therefore, it seems that there exists a threshold roughness, in our case slightly larger than 10 nm, impacting both the static water and hexadecane CAs. Our results clarified that when roughness reaches the threshold, there is a burst in static water and hexadecane CAs, which plateau for further increased hot water treatment times.

The methanol CAs are found to be quite different from both water and hexadecane: they practically remain at the same level with fluctuations (57 ± 3°), regardless of treatment time. The reason why the surface roughness had almost no impact on the wettability of methanol might be due to the stronger spreading of methanol on the surface. This is most likely caused by its lower surface tension (22–23 mN m^{-1}) in comparison with those of hexadecane (27–28 mN m^{-1}) and water (72.8 mN m^{-1}). Methanol molecules would fill the pores of the FPA/Al surface to squeeze out air so that the differences in roughness as found in our system do not make a difference in determining its CAs.

In order to study the thermal stability of the FPA/Al surfaces, water CAs of FPA SAMs prepared on Al films treated in hot water for 120 s were examined. Figure 9 shows water CAs of FPA/Al samples annealed at 100–400°C, where the data of the control (i.e. the sample without annealing) are also shown as the reference.

As shown in Figure 9, in comparison with the control, the 100°C annealed sample has a small amount of increase in its static water CAs, from 166° to 169°. The hysteresis between the advancing and receding CAs is now only 3°, a significant decrease from that of the control (~10°), indicating an improvement of hydrophobicity. The static CAs and the hysteresis between the advancing and receding CAs remain constant for samples annealed at 100–300°C. When annealed at 350°C, while the advancing CA is still high (163°), the static and receding CAs were now 147° and 99°, which are significantly lower than their counterparts in the 300°C case. The significant increase in the hysteresis between advancing and receding CAs indicates degradation of the hydrophobicity of the FPA SAMs upon annealing at 350°C. When the annealing temperature was raised to 400°C, the static CA was only 17°, with the advancing CA being 28° and receding CA practically zero. Therefore, the surface became hydrophilic when annealed at 400°C, a reflection of the presence of an oxidized surface.

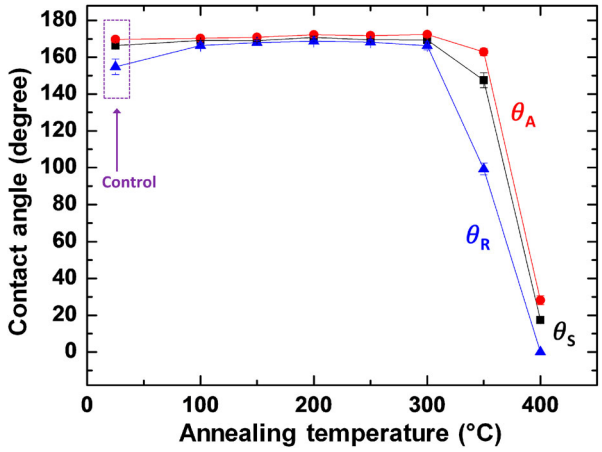

Figure 9. Static, advancing and receding water contact angles as a function of annealing temperature for FPA SAMs prepared on an Al film treated in hot water for 120 s.

The CAs shown in Figure 9 are useful for us to understand the surface chemistry associated with the thermal stability of the SAMs. The experimental observation that annealing at 100°C improved the hydrophobicity of the SAMs suggests that there are further reactions between the headgroups of FPA and the Al substrate, leading to an improved ordering of the FPA monolayer. This is reasonable for FPA because the phosphonic acid headgroup can be anchored to the Al substrate via a mono-, bi-, or tridentate bond configuration [40]. The results shown in Figure 9 thus suggest that the molecules form either mono- or bidentate bonds when FPA molecules self-assemble on the Al surface at room temperature, while annealing at 100°C promotes further reaction leading to the formation of either bi- or tridentate bonds. As a result, the hydrophobicity of the FPA SAMs is enhanced.

Further increases in annealing temperature would not impact the headgroup-substrate interaction if tridentate bonds are in place for all molecules. At the same time, with increased annealing temperatures, the fluoroalkyl chains and the two CH_2 groups of the FPA molecules will be degraded. This is clearly shown when annealing temperature was raised to 350°C, where the hydrophobicity of FPA SAMs was degraded. When further increasing the annealing temperature to 400°C, the surface of the sample becomes hydrophilic.

Since the FPA molecules were anchored to the Al film via P–O–Al covalent bonds, it is more likely that the removal or oxidation of fluoroalkyl chains was responsible for the increased hydrophilicity of the FAP/Al samples with annealing temperatures beyond 300°C, especially when the annealing experiment was conducted in air. In order to further understand the surface chemistry of FPA SAMs subjected to annealing, TOF-SIMS was employed to follow the chemistry of the FPA SAMs derivatized on Al surfaces as a function of annealing temperature.

The chemistry of the FPA/Al surfaces

Figure 10 shows the negative secondary ion mass spectra obtained on FPA powder (referred to as free FPA), the control and FPA/Al samples annealed at 150, 350 and 400°C. The data for samples annealing at 100, 200, 250, and 300°C are omitted for clarity purposes. The Al film used was treated in hot water for 120 s. For the free FPA, as shown in Figure 10(a,b), the most abundant negative ion fragments are F^-(m/z 19), F_2^- (38), PO_2^- (63), PO_3^- (79) and PO_3H^- (80).

We noticed that PO_3H^- is a reflection of free OPA powder, as well as OPA SAMs on a silicon substrate where the headgroup is anchored to the substrate via hydrogen-bonding [46]. In other words, this is a

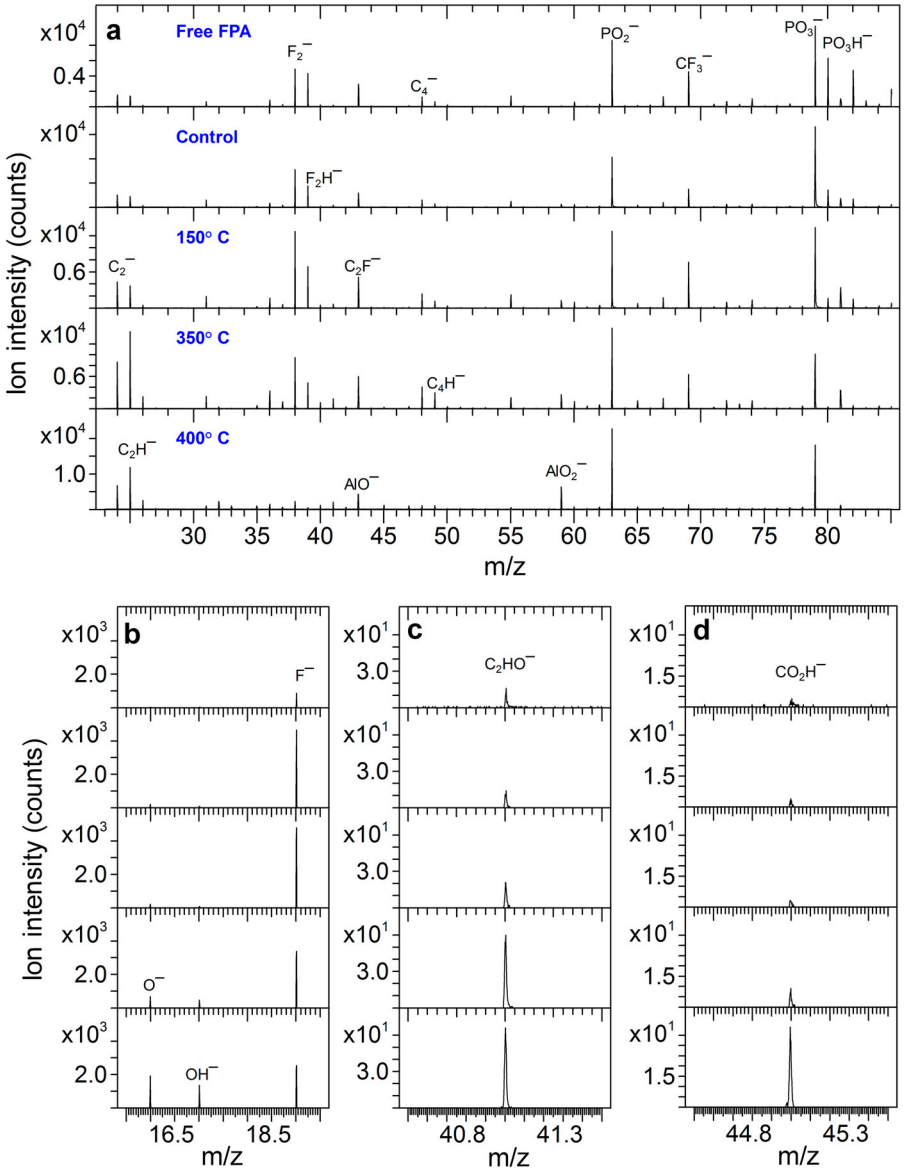

Figure 10. Negative secondary ion mass spectra in m/z 11–85 (a) of free FPA, the control and annealed FPA SAMs on Al films annealed at different temperatures. For clarity purposes, shown in this figure are samples annealed at 150, 350 and 400°C, while those annealed at 100, 200, 250 and 300 °C are omitted. The Al film used for this set of measurements was treated in hot water for 120 s. Spectra in (b)–(d) show increases of intensities of O^- and OH^- (b), C_2HO^- (c) and CO_2H^- (d), respectively.

reflection of the presence of OH functional groups in the molecular headgroups, meaning that condensation reaction is possible. As shown in Figure 10(a), on the FPA SAMs, the PO_3H^- intensity reduces greatly for FPA SAMs in comparison with their free molecules. We noticed that with increased annealing temperatures, the PO_3H^- intensity becomes less and less.

Figure 10(b) shows the increase of O^- (16) and OH^- (17) intensities when annealing temperatures were raised to 350 and 400°C. As indicators of oxidation of the two CH_2 groups in FPA, C_2HO^- (41) and CO_2H^- (45) are shown in Figure 10(c,d), respectively. From these figures, one can see that the increase in C_2HO^- intensity is much more at 350°C than those of O^-, OH^- and CO_2H^-, whose intensities increase significantly at 400°C.

C_2HO^- and CO_2H^- are major species indicative of oxidation of alkyl chains. These two species are common fragments detected from organic molecules containing carboxylates and esters [29,31]. The observed increases in their intensities indicate the two CH_2 groups in each of an FPA molecule were oxidized at elevated temperatures.

Shown in Figure 11 are positive secondary ion counterparts of what are shown in Figure 10. Figure 11(a) shows abundant CF^+ (31), CF_2^+ (50), CF_3^+ (69), $C_3F_3^+$ (93), $C_2F_4^+$ (100), $C_2F_5^+$ (119) and $C_3F_5^+$ (131), which are characteristic ions of perfluorocarbons. For the free FPA powder, abundant PO^+ (47) and $PO_2H_2^+$ (65) are also observed. These two ions are much weaker from FPA SAMs on the Al film.

With increased annealing temperatures, the higher mass $C_xF_y^+$ ions become weaker. For example, at 350° C, only CF_3^+ have a decent abundance, while at 400° C only minimal CF^+ was detected. As shown in Figure 11(b), this corresponds to increased Al^+ abundance,

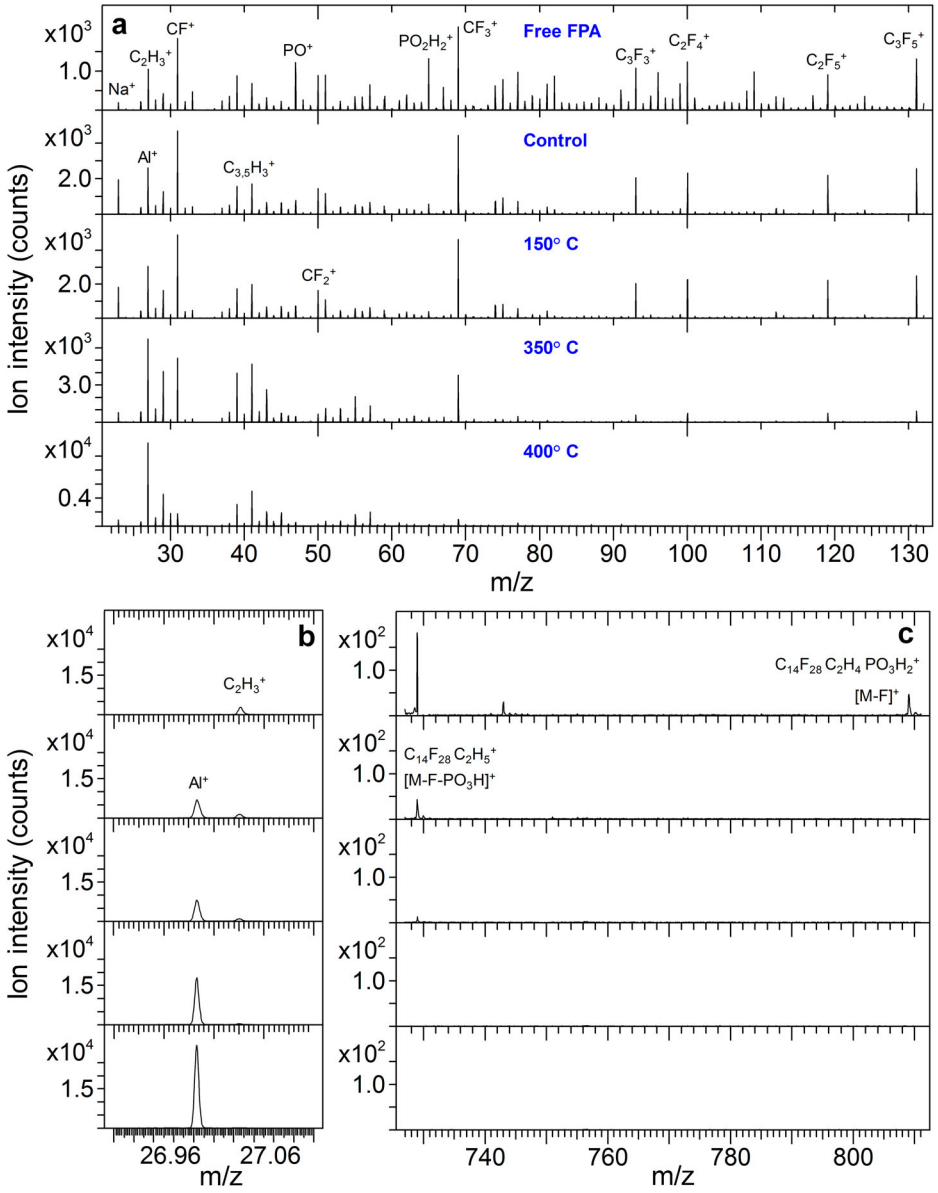

Figure 11. Positive secondary ion mass spectra in m/z 22–132 (a) of free FPA, the control and annealed FPA SAMs on Al films annealed at different temperatures. For clarity, shown in this figure are samples annealed at 150, 350 and 400°C, while those annealed at 100, 200, 250 and 300°C are omitted. The Al films used for this set of measurements were treated in hot water for 120 s. Signals of Al^+ for the FPA samples are shown in (b). As shown in (c), the de-fluorine molecular ion $C_{14}F_{28}C_2H_4PO_3H_2^+$, or $[M–F]^+$, is detected from free FPA powder, but absent from FPA SAMs on Al surfaces. The peak at m/z 729 is assigned to $C_{14}F_{28}$-$C_2H_5^+$ or $[M–F–PO_3H]^+$, which is the fluoroalkyl chain of the molecule with the removal of the phosphonic acid headgroup and a fluorine atom, as well as with the capture of a hydrogen atom.

indicating that the perfluorocarbons of the FPA molecules are being degraded/removed when annealed at these elevated temperatures.

It is interesting to note that unlike alkylphosphonic acids (e.g. OPA), no hydrogenated molecular ion is detected from the FPA. Instead, as shown in Figure 11(c), we detected a peak at m/z 809 from the free FPA powder alone, which is assigned to $C_{14}F_{28}C_2H_4PO_3H_2^+$ or $[M–F]^+$, with M representing the FPA molecular formula of $C_{14}F_{29}C_2H_4PO_3H_2$, The lack of this ion from FPA SAMs on Al films suggests that FPA molecules are anchored to Al films by P–O–Al bonds and cannot be fragmented (by the bombardment of the energetic primary ion beam) as a molecular ion, a reflection of an excellent bonding strength [47] between the FPA molecular headgroup and the Al substrate.

The peak at m/z 729 shown in Figure 11(c) is identified as $C_{14}F_{28}C_2H_5^+$, or $[M–F–PO_3H]^+$. This ion is thus the fluoroalkyl chain of the FPA molecule with the removal of a fluorine atom and with the phosphonic headgroup replaced by a hydrogen atom. This ion may serve as a marker for alteration of the FPA molecules upon annealing.

Figure 12 presents the intensities of PO_2^-, PO_3^-, Al^+, CF_3^-, $C_2H_3^+$, O^-, OH^-, PO_3H^-, CO_2H^- and $C_{14}F_{28}C_2H_5^+$ or $[M–F–PO_3H]^+$ obtained from the control and FPA/Al samples annealed at temperatures

100–400°C. There are no significant changes in intensities of PO_2^- and PO_3^- upon annealing. These two ions are characteristic of the FPA molecular headgroups and are not informative in studying degradation of molecules upon annealing [29,31]. Nevertheless, their behaviour indicates that the phosphonate groups remained largely unchanged on the Al substrate even upon annealing at 400°C.

The $[M–F–PO_3H]^+$ ion is a sensitive marker for studying intact fluoroalkyl chains of the FPA molecules. This is because any changes, such as oxidation, cross-linking or scissoring occurred to any portion of the molecular chain will prevent it from being fragmented as $[M–F–PO_3H]^+$. As shown in Figure 12, for the sample annealed at 100°C, the $[M–F–PO_3H]^+$ intensity decreased significantly, down to 35% of that of the control. Because the chemical structure of the molecular chains cannot be altered at this temperature, the drastic decrease in $[M–F–PO_3H]^+$ intensity has to be attributed to physical changes induced by annealing at 100°C. The most possible physical changes include enhanced packing density and ordering of the fluoroalkyl chains induced by annealing. If we assume that the bonding configuration is not tridentate [40] for all FPA molecules in the as-prepared sample (i.e. the control), then the free OH groups left in FPA molecules will be available for further reactions between them and the Al substrate to form more P–O–Al bonds.

Therefore, our wettability studies and TOF-SIMS analyses hint that even more closely packed chains likely reduces the yield of $[M–F–PO_3H]^+$. Another possibility for the decreasing $[M–F–PO_3H]^+$ intensity with increased annealing temperature is that the two CH_2 groups of fluoroalkyl chains may be oxidized, resulting in reduced abundance of the ion. It is highly possible that the degradation of the two CH_2 groups alters the chemical structure of the fluoroalkyl chains without undermining the structure integrity of the SAMs. This hypothesis would then explain why the $[M–F–PO_3H]^+$ intensity decreased while the superhydrophobicity was maintained when the FPA SAMs were annealed at 100–300°C.

As shown in Figure 12, it is intriguing that the intensity of $C_2H_3^+$ decreases with increased annealing temperature. This leads us to believe that $C_2H_3^+$ might be a usable indicator for the two CH_2 groups connecting the phosphonate headgroup and the perfluorocarbon chain. We thus infer that both possibilities, one physical and the other chemical, coexist, with the physical change (i.e. the ordering of the molecular chains) being dominant at lower and the chemical change (oxidation of the alkyl portion) at higher annealing temperatures, respectively.

It has been noticed that PO_3H^- is an indicator for OH group(s) in organophosphonic acid [42]. As shown in Figure 12, this ion decreased with increased annealing temperatures. We infer that this may be a reflection of increased tridentate bonds between the FPA molecule and the substrate for samples annealed at temperatures up to 300°C, which showed superhydrophobicity as evidenced in Figure 9. For annealing temperatures beyond 300°C, degradation of the fluoroalkyl chains occurred, eventually changing the superhydrophobic surface to a hydrophilic one.

It is worth noting that we have identified species useful in revealing oxidation of the alkyl portion of the FPA molecules, which are O^-, OH^-, C_2HO^- and CO_2H^- [29]. The Intensities of these species increased by an order of magnitude when the annealing temperature was beyond 300°C, signalling the start of oxidations of the molecule. It agrees well with the drastic decrease observed in CF_3^- intensity. This suggests that the perfluoracarbon portion of FPA is removed from the surface when annealing temperatures were raised beyond 300°C, resulting in significant increases in Al^+ intensities.

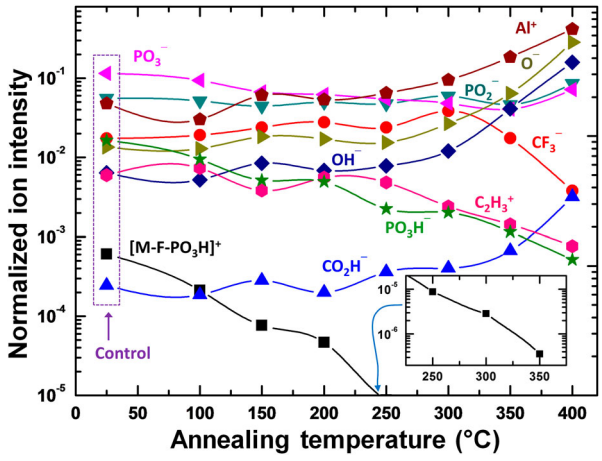

Figure 12. Selected ion intensities normalized to total ion intensity for FPA SAMs on Al as a function of annealing temperature. The data for the control (i.e. without annealing) are indicated in the figure. The insert is the same curve of $[M–F–PO_3H]^+$ in the range of annealing temperatures 220–400°C. The standard deviations for all data are up to several per cent (not shown).

Conclusions

We have demonstrated a simple methodology to render superhydrophobicity via derivatization of a fluoroalkyl phosphonic acid (FPA), $CF_3(CF_2)_{13}(CH_2)_2P(=O)(OH)_2$, on an Al surface briefly treated in hot water for creating a roughened surface. Nano-structured Al surfaces were achieved by roughening sputter-deposited Al films on a Si wafer via de-ionized water treatment at 90°C. The roughness surged 40 times of that of the control for Al films treated in hot water for 30–40 s and plateaued thereafter. We found that briefly treated (e.g. 50 s) samples have flat islands on the surface, while for those treated for prolonged times (e.g. 720 s) the surface was characterized by

funnel-like features. Moreover, it was found that a 15-nm Al film, when subjected to hot water treatment for 50 s and beyond, grew to a porous one with its thickness reaching ~200 nm.

When derivatized with SAMs of FPA, all the Al films, regardless of their roughness, were rendered hydrophobic. However, superhydrophobicity was achieved only on Al films treated in hot water for 50–180 s. This observation indicates that the probing water droplet is in the Cassie–Baxter regime, which is supported by the morphology of Al films characterized by their porosity and flat-island like features that would prevent water from entering the pores (thus leaving air there to also support the water droplet). Our results of contact angle measurements and TOF-SIMS analyses revealed that the FPA SAMs on a roughened Al film has excellent thermal stability: its superhydrophobicity was not degraded until annealing temperatures were beyond 300°C. We also observed enhancement in hydrophobicity and bonding strength upon annealing at 100°C, hinting further reactions between the FPA headgroups and the Al surface.

On the other hand, for FPA SAMs prepared on Al films treated for 240–720 s, the receding contact angles decreased significantly in comparison with their 50–180 s counterparts, though the static and advancing contact angles remained the same for both groups. This reveals that the surface morphology of the Al films treated for 240–720 s does not render superhydrophobicity, likely due to the funnel-like features observed on the Al films subjected to prolonged hot water treatment, which leads to Wenzel regime of the probing water droplet as it would enter these relatively open pores.

Acknowledgement

YMH is grateful to Professor David Shoesmith, the Director of Surface Science Western, for his kind help and encouragement during the visit to the lab.

Disclosure statement

No potential conflict of interest was reported by the authors.

Funding

This work was partially supported by China Scholarship Council and Natural Science Foundation of China (NSFC) [grants number 11564002 and 11764003].

ORCID

Heng-Yong Nie http://orcid.org/0000-0002-8287-5171

References

[1] Zheng SL, Li C, Fu QT, et al. Development of stable superhydrophobic coatings on aluminum surface for corrosion-resistant, self-cleaning, and anti-icing applications. Mater Des. 2016;93:261–270.
[2] Peng S, Deng WL. A simple method to prepare superamphiphobic aluminum surface with excellent stability. Colloids Surf A. 2015;481:143–150.
[3] Liao RJ, Zuo ZP, Guo C. Fabrication of superhydrophobic surface on aluminum by continuous chemical etching and its anti-icing property. Appl Surf Sci. 2014;317:701–709.
[4] Saifaldeen ZS, Khedir KR, Cansizoglu MF. Superamphiphobic aluminum alloy surfaces with micro and nanoscale hierarchical roughness produced by a simple and environmentally friendly technique. J Mater Sci. 2014;49:1839–1853.
[5] Liu CS, Su FH, Liang JZ. Facile fabrication of a robust and corrosion resistant superhydrophobic aluminum alloy surface by a novel method. RSC Adv. 2014;4:55556–55564.
[6] Palanivel R, Mathews PK, Murugan N, et al. Effect of tool rotational speed and pin profile on microstructure and tensile strength of dissimilar friction stir welded AA5083-H111 and AA6351-T6 aluminum alloys. Mater Des. 2012;40:7–16.
[7] Jiang XL, Wang SH, Zhang ZJ. Study on AC flashover performance and discharge process of polluted and iced IEC standard suspension insulator string. IEEE Trans Power Del. 2007;22:472–480.
[8] Farzaneh M, Drapeau JF. AC flashover performance of insulators covered with artificial ice. IEEE Trans Power Del. 1995;10:1038–1051.
[9] Fikke SM, Hanssen JE, Rolfseng L. Long range transported pollutants and conductivity of atmospheric ice on insulators. IEEE Trans Power Del. 1993;8:1311–1321.
[10] Jeong CY, Choi CH. Single-step direct fabrication of pillar-on-pore hybrid nanostructures in anodizing aluminum for superior superhydrophobic efficiency. ACS Appl Mat Interf. 2012;4:842–848.
[11] Ji SM, Ramadhianti PA, Nguyen TB, et al. Simple fabrication approach for superhydrophobic and superoleophobic Al surface. Microelectron Eng. 2013;111:404–408.
[12] Li XM, Reinhoudt D, Crego-Calama M. What do we need for a superhydrophobic surface? A review on the recent progress in the preparation of superhydrophobic surfaces. Chem Soc Rev. 2007;36:1350–1368.
[13] Hu YM, Zhu Y, Zhou W, et al. Dip-coating for dodecylphosphonic acid derivatization on aluminum surfaces: an easy approach to superhydrophobicity. J Coat Technol Res. 2016;13:115–121.
[14] Zhu Y, Hu YM, Nie HY, et al. Superhydrophobicity via organophosphonic acid derivatised aluminium films. Surf Eng. 2016;32:114–118.
[15] Xu WJ, Song JL, Sun J, et al. Fabrication of superhydrophobic surfaces on aluminum substrates using NaNO3 electrolytes. J Mater Sci. 2011;46:5925–5930.
[16] Wu YP, Zhang CY. Analysis of anti-condensation mechanism on superhydrophobic anodic aluminum oxide surface. Appl Therm Eng. 2013;58:664–669.
[17] Bernagozzi I, Antonini C, Villa F, et al. Fabricating superhydrophobic aluminum: An optimized one-step wet synthesis using fluoroalkyl silane. Colloids Surf A. 2014;441:919–924.

[18] Li PP, Chen XH, Yang GB, et al. Fabrication and characterization of stable superhydrophobic surface with good friction-reducing performance on Al foil. Appl Surf Sci. 2014;300:184–190.
[19] McHale JM, Auroux A, Perrotta AJ, et al. Surface energies and thermodynamic phase stability in nanocrystalline aluminas. Science. 1997;277:788–791.
[20] Melo-Espinosa EA, Sánchez-Borroto Y, Errasti MI, et al. Surface tension prediction of vegetable oils using artificial neural networks and multiple linear regression. Energy Proc. 2014;57:886–895.
[21] Song JL, Huang S, Hu K, et al. Fabrication of superoleophobic surfaces on Al substrates. J Mater Chem A. 2013;1:14783–14789.
[22] Wang L, Yang JY, Zhu Y, et al. An environment-friendly fabrication of superhydrophobic surfaces on steel and magnesium alloy. Mater Lett. 2016;171:297–299.
[23] Wang L, Yang JY, Zhu Y, et al. A study of the mechanical and chemical durability of ultra-Ever Dry superhydrophobic coating on low carbon steel surface. Colloids Surf A. 2016;497:16–27.
[24] Zhu Y, Hu YM, Ma L, et al. Ultra-repellency of Al surfaces: design and evaluation. J Coat Technol Res. 2018;15:633–641.
[25] Saadi NS, Hassan LB, Karabacak T. Metal oxide nanostructures by a simple hot water treatment. Sci. Rep. 2017;7:7158.
[26] Feng LB, Che YH, Liu YH, et al. Fabrication of superhydrophobic aluminium alloy surface with excellent corrosion resistance by a facile and environment-friendly method. Appl Surf Sci. 2013;283:367–374.
[27] Liakos IL, Newman RC, McAlpine E, et al. Study of the resistance of SAMs on aluminium to acidic and basic solutions using dynamic contact angle measurement. Langmuir. 2007;23:995–999.
[28] Luschtinetz R, Oliveira AF, Frenzel J, et al. Adsorption of phosphonic and ethylphosphonic acid on aluminum oxide surfaces. Surf Sci. 2008;602:1347–1359.
[29] Chen DH, Wu HKY, Naderi-Gohar S, et al. An extremely rapid dip-coating method for self-assembly of octadecylphosphonic acid and its thermal stability on an aluminum film. J Mater Chem C. 2014;2:9941–9948.
[30] Hoque E, DeRose JA, Hoffmann P, et al. Alkylperfluorosilane self-assembled monolayers on aluminum: a comparison with alkylphosphonate self-assembled monolayers. J Phys Chem C. 2007;111:3956–3962.
[31] Nie HY. Oxidizing octadecylphosphonic acid molecules without disrupting their self-assembled monolayers. Anal Methods. 2013;5:4911–4920.
[32] Hoque E, DeRose JA, Hoffmann P, et al. Robust perfluorosilanized copper surfaces. Surf Interface Anal. 2006;38:62–68.
[33] Somlo B, Gupta V. A hydrophobic self-assembled monolayer with improved adhesion to aluminum for deicing application. Mech Mater. 2001;33:471–480.
[34] Hansal WEG, Hansal S, Pölzler M, et al. Investigation of polysiloxane coatings as corrosion inhibitors of zinc surfaces. Surf Coat Technol. 2006;200:3056–3063.
[35] Nie HY, McIntyre NS. A simple and effective method of evaluating atomic force microscopy tip performance. Langmuir. 2001;17:432–436.
[36] Rider AN, Arnot DR. Boiling water and silane pretreatment of aluminium alloys for durable adhesive bonding. Int J Adhes Adhes. 2000;20:209–220.
[37] Jafari R, Farzaneh M. Fabrication of superhydrophobic nanostructured surface on aluminum alloy. Appl Phys A. 2011;102:195–199.
[38] Deng R, Hu YM, Wang L, et al. An easy and environmentally-friendly approach to superamphiphobicity of aluminum surfaces. Appl Surf Sci. 2017;402:301–307.
[39] Alwitt RS. The aluminum-water system. In: Diggle JW, Vijh AK, editors. Oxides and oxide films. New York (NY): Marcel Dekker; 1976. p. 169.
[40] Bulusu A, Paniagua SA, MacLeod BA, et al. Efficient modification of metal oxide surfaces with phosphonic acids by spray coating. Langmuir. 2013;29:3935–3942.
[41] Vedder W, Vermilyea DA. Aluminum + water reaction. Trans Faraday Soc. 1969;65:561–584.
[42] Hozumi A, Kim BY, McCarthy TJ. Hydrophobicity of perfluoroalkyl isocyanate monolayers on oxidized aluminum surfaces. Langmuir. 2009;25:6834–6840.
[43] Saifaldeena ZS, Khedir KR, Camci MT. The effect of polar end of long-chain fluorocarbon oligomers in promoting the superamphiphobic property over multiscale rough Al alloy surfaces. Appl Surf Sci. 2016;379:55–65.
[44] Cassie ABD, Baxter S. Wettability of porous surfaces. Trans Faraday Soc. 1944;40:546–551.
[45] Wenzel RN. Surface roughness and contact angle. J Phys Chem. 1949;53:1466–1467.
[46] Nie HY. Self-assembled monolayers of octadecylphosphonic acid and polymer films: surface chemistry and chemical structures studied by time-of-flight secondary ion mass spectrometry. Surf Interface Anal. 2017;49:1431–1441.
[47] Nie HY. Revealing different bonding modes of self-assembled octadecylphosphonic acid monolayers on oxides by time-of-flight secondary ion mass spectrometry: silicon vs aluminum. Anal Chem. 2010;82:3371–3376.